Spatially heterogeneous dynamics in a two-dimensional glass-forming binary mixture

1998 J. Phys.: Condens. Matter 10 10115

(http://iopscience.iop.org/0953-8984/10/45/002)

J. Phys.: Condens. Matter **10** (1998) 10115–10134. Printed in the UK PII: S0953-8984(98)96470-0

Spatially heterogeneous dynamics in a two-dimensional glass-forming binary mixture

Donna N Perera†

Aperiodic Solids Research Team, National Research Institute for Metals (NRIM), 1-2-1 Sengen, Tsukuba, Ibaraki 305, Japan

Received 4 August 1998, in final form 8 September 1998

Abstract. A quantitative analysis is presented of the increasing degree of dynamical correlations with decreasing temperature in a fragile glass-former consisting of a two-dimensional binary mixture of soft discs with a diameter ratio of $\sigma_2/\sigma_1 = 1.4$. The analysis involves a study of the spatial distribution of local relaxation times, defined as the time taken for each particle to first travel a distance r from its initial position. For the binary mixture, a temperature-independent optimum value of $r \approx \sigma_1$ is found to maximize the spatial segregation of particles into different kinetic domains. The regions of 'fast' and 'slow' particles grow in size as the system is cooled, indicating an increasing degree of cooperativity in the particle dynamics. A measure of the linear dimensions of these clusters is provided. It is shown that only 'slow' subsets of particles are caged on intermediate timescales and that the lifetime of these slow domains increases dramatically with decreasing temperature in the supercooled mixture. A substantial decay in the incoherent scattering functions can still be accomplished, however, on these timescales, despite the relative immobility of a significant fraction of the system. A further observation is a change in the manner in which relaxation progresses throughout the system with cooling. At high temperatures the initially fast relaxing sites are randomly distributed throughout the system, whereas at low temperatures they tend to be clumped together. This subsequently results in a less homogeneous progression of relaxation at the lower temperatures, since relaxation proceeds primarily by radiating outwards from existing fast centres.

1. Introduction

A consequence of the enhancement of cooperativity in particle motion with supercooling is an increasingly coarser spatial fragmentation of the system under study into regions that differ from one another in average relaxation rates. Such dynamical heterogeneity now appears to be a common characteristic of fragile glass-forming materials, as many laboratory experiments [1–4] and computer simulation studies [5–12] have substantiated.

In the present work, an investigation of the natural development of such kinetic inhomogeneities in a specific system: a two-dimensional (2D) fragile glass-former, is carried out via molecular dynamics (MD) simulations, in order to understand why below a certain intermediate temperature, there is a dramatic slowing down of structural relaxation beyond that attributed to the simple loss of thermal energy with decreasing temperature. A preliminary report of this work can be found in reference [9]. The system consists of an equimolar binary mixture of soft discs with a diameter ratio of $\sigma_2/\sigma_1 = 1.4$. The 2D mixture has been chosen for the ease with which the spatial extent of dynamical

† E-mail: dperera@tamamori.nrim.go.jp.

0953-8984/98/4510115+20$19.50

correlations can be visualized, as well as for its amenability to computer simulation. This binary mixture exhibits many of the characteristics of glassy relaxation observed in real and simulated fragile glass-formers, such as stretched exponential and two-step decay of relaxation functions, non-Arrhenius temperature dependence of relaxation times and a substantial drop in the heat capacity at the computer glass transition temperature [10–14]. Comprehensive analyses of the structural and dynamical aspects of this system are presented elsewhere [13, 14].

The procedure used to obtain the spatial distribution of relaxation times for the binary mixture is the one introduced by Hurley and Harrowell [15] in their quantitative analysis of the kinetic structure in a single-component 2D liquid of soft discs. They defined the local relaxation time τ_r of a given particle as the time taken by that particle to first move a distance r from its initial position, i.e. the first passage time. Once the distribution of τ_r is known, the particles can then be arbitrarily partitioned into 'fast' and 'slow' groups. Hurley and Harrowell have shown that for the pure 2D liquid at a constant temperature, there is a well-defined density-independent optimum value for r which maximizes the spatial segregation of the fast and slow particles in the liquid. This value is $r \approx 0.8\sigma_1$. For the 2D binary mixture, we find that the optimum distance for maximizing the resolution of the kinetic structure is $r \approx \sigma_1$. Details are provided in section 3.

By fixing the cut-off distance r at σ_1 and monitoring the change in the spatial distribution of the relaxation times as a function of temperature, we observe that at relatively high temperatures, the slow and fast particles are randomly distributed throughout the system with only a small degree of clustering into domains of similar mobility. However, as the temperature is lowered, there is an increasing degree of spatial heterogeneity in the particle dynamics, with the linear dimensions of the slow domains (and complementarily, the fast domains, due to exclusion) increasing in size. By resolving the contributions of the slow and fast factions of particles to the mean squared displacement (MSD), we have also observed that *only* the slow particles are 'caged', as is evident from the plateau in the MSD for this contribution, on timescales that at some of the low temperatures that we have investigated extend to several orders of magnitude longer than the average collision time t_c in the mixture, which is defined to be the time at which the velocity autocorrelation function first crosses zero. This collision time is only very weakly dependent on temperature in the liquid, supercooled liquid and amorphous states. During the lifetime of the caged particles, the incoherent scattering functions are observed to have decayed by more than 80% except at the very lowest temperatures. These results are presented in section 4.

A change in relaxation mechanism also occurs as the system is cooled. This can be visualized as follows. We define a particle as having relaxed its local structure if it has first moved a distance $r \geqslant \sigma_1$ by a certain time. By plotting the positions of successively greater numbers of the fastest particles, the progression of relaxation throughout the system can be followed. We observe that at relatively high temperatures in the liquid state, the initially fast relaxing sites appear randomly throughout the mixture. As time progresses, relaxation proceeds by propagation outwards from these existing sites and also by spontaneous emergence of new relaxing centres in previously slow domains. In the dense low-temperature mixtures, however, the first few fastest particles tend to be clumped together rather than being randomly distributed. The spreading of relaxation outwards from these initially clustered fast sites then results in a less spatially homogeneous distribution of relaxation. These results which are described in section 5 are another clear representation of the increasing degree of cooperativity in particle dynamics at relatively high densities.

2. Model and computational details

We have carried out a series of MD simulations on a 2D system consisting of an equimolar ($x_1 = N_1/N = 0.5$) mixture of two types of particle with diameters $\sigma_2 = 1.4$ and $\sigma_1 = 1$, but with the same mass m. The three pairwise-additive interactions are given by the purely repulsive soft-core potentials:

$$u_{ab}(r) = \epsilon \left[\frac{\sigma_{ab}}{r}\right]^{12} \qquad a, b = 1, 2 \tag{1}$$

where $\sigma_a = \sigma_{aa}$ and $\sigma_{ab} = (\sigma_a + \sigma_b)/2$. The cut-off radii of the interactions were chosen to be $4.5\sigma_{ab}$. The units of mass, length and time are m, σ_1 and $\tau = \sigma_1\sqrt{m/\epsilon}$ respectively. A total of $N = 1024$ particles were enclosed in a square box with periodic boundary conditions. The simulations were carried out at constant number of particles, pressure ($P^* = P\sigma_1^2/\epsilon$) and temperature ($T^* = k_B T/\epsilon$, where k_B is Boltzmann's constant), using the constraint MD algorithm of Evans and Morriss [16, 17] in which the instantaneous temperature and pressure are strict constants of the motion. A third-order (four-value) Gear predictor–corrector algorithm was used to integrate the equations of motion [17]. The time steps employed were 0.0025τ for $T^* > 1$ and 0.005τ for $T^* \leqslant 1$. For argon units of $\epsilon = 120k_B$, $m = 6.6 \times 10^{-23}$ g and $\sigma_1 = 3.4$ Å, these time steps correspond to approximately five and ten femtoseconds respectively. The pressure was fixed at $P^* = 13.5$ and states at 16 different reduced temperatures in the range $T^* \in [0.1, 5]$ were simulated. For this pressure, the freezing temperatures of the monocomponent 2D liquid of small and large particles are

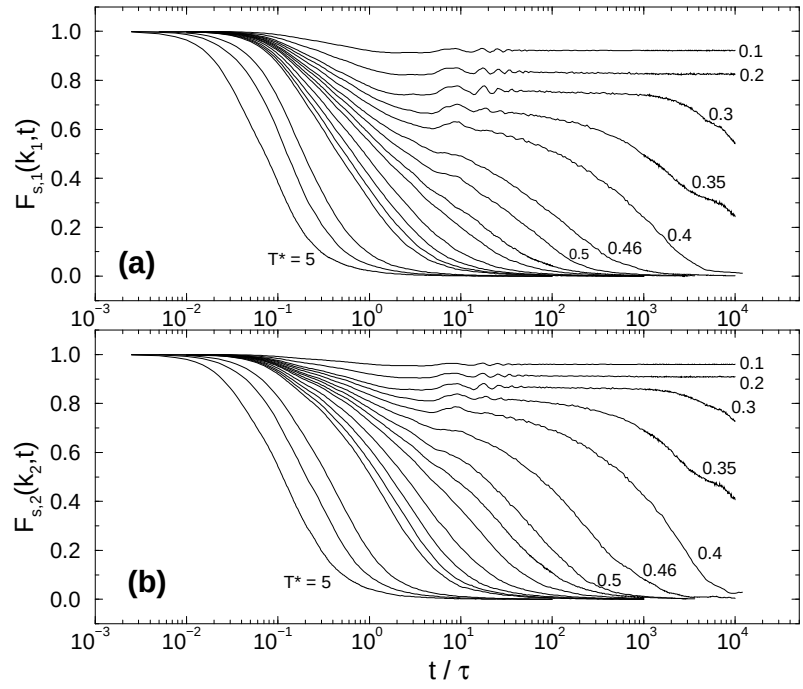

Figure 1. The incoherent scattering functions $F_{s,1}(k_1, t)$ and $F_{s,2}(k_2, t)$ of the small (top figure) and large (bottom figure) particles respectively calculated at the wave vector corresponding to the position of the first maximum in the respective partial structure factors. The wave vectors have magnitudes of $k_1 = 7.17\sigma_1^{-1}$ and $k_2 = 5.60\sigma_1^{-1}$. From left to right the curves correspond to $T^* = 5$, 3, 2, 1, 0.9, 0.8, 0.7, 0.6, 0.55, 0.5, 0.46, 0.4, 0.35, 0.3, 0.2, 0.1.

$T^*_{f,1} = 0.95$ and $T^*_{f,2} = 1.70$ respectively. Full details of the simulations are provided in reference [13].

In order to demonstrate at which temperature the system is able to reach equilibrium within our simulation time window, we show in figure 1 the spectrum of incoherent scattering functions,

$$F_{s,a}(k,t) = \frac{1}{N_a}\left\langle \sum_{j=1}^{N_a} \exp\left\{ \mathrm{i}\boldsymbol{k}\cdot[\boldsymbol{r}_j(t) - \boldsymbol{r}_j(0)]\right\}\right\rangle \qquad a = 1, 2 \tag{2}$$

for both particle species. The angular brackets denote an average over time origins and an angular average over the directions of the wave vector $\boldsymbol{k}$. The magnitude of $\boldsymbol{k}$ was chosen to be $k_1 = 7.17\sigma_1^{-1}$ for $F_{s,1}(k,t)$ and $k_2 = 5.60\sigma_1^{-1}$ for $F_{s,2}(k,t)$. These correspond to the positions of the first peak maximum in the respective partial structure factors, which are only very weakly dependent on temperature. Figure 1 shows that the scattering functions are able to decay to zero for $T^* \geqslant 0.4$. Below $T^* = 0.4$, structural relaxation cannot fully proceed to equilibrium due to the finite timescale of the simulations. Thus, the computer glass transition temperature T^*_g for these simulations, defined as the temperature at which the system is no longer able to relax completely to equilibrium, lies between $T^* = 0.4$ and 0.3.

Another feature worth noticing in figure 1 is the two-step decay process of the relaxation functions at the lower temperatures. The step is first observed at $T^* \approx 0.5$. This temperature will be denoted as a 'crossover' temperature T^*_c to mark the perceived change in the dynamics of the system at this temperature, such as the start of the departure of the structural relaxation times with decreasing temperature from their high-temperature Arrhenius dependence. The structural relaxation times here are defined to be the times taken by the incoherent and intermediate scattering functions to decay to $1/e$ of their initial values. Other dynamical changes at T^*_c are described in references [10, 11, 12, 14]. In section 5 we shall demonstrate explicitly that there is a change in relaxation mechanism in going from above to below T^*_c. This is not surprising since the appearance of the second slower relaxation process at T^*_c in figure 1 denotes the start of a rapidly increasing separation in timescales between fast and slow relaxation with decreasing temperature.

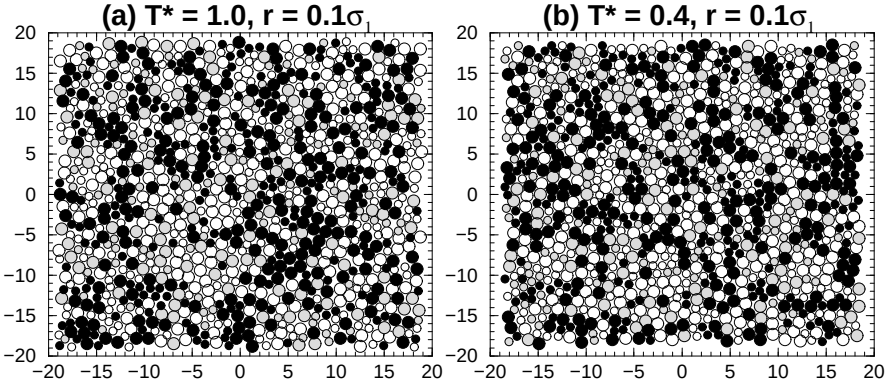

Figure 2. Representative spatial relaxation time maps at (a) $T^* = 1$ and (b) $T^* = 0.4$ for a cut-off distance of $r = 0.1\sigma_1$. The circles represent the particle positions at an initial time. The fastest 40% of particles are shown by the unfilled circles, the intermediate 20% are shaded grey and the slowest 40% are black. The particles are not drawn to scale.

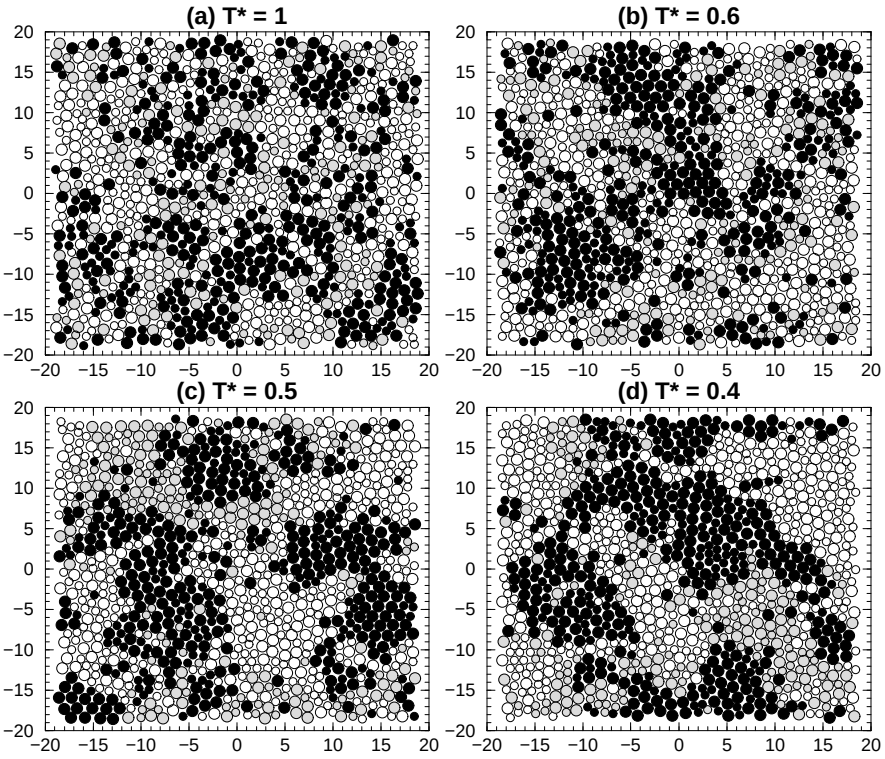

Figure 3. Representative spatial relaxation time maps at (a) $T^* = 1$, (b) $T^* = 0.6$, (c) $T^* = 0.5$ and (d) $T^* = 0.4$ for a cut-off distance of $r = \sigma_1$. The key is the same as for figure 2. Observe the increase in the clustering of the slow particles (black circles) in going from $T^* = 1$ to 0.4.

3. Kinetic analysis

3.1. Resolving the kinetic structure

We define a local relaxation time $\tau_r(i)$ of a given particle i to be the time that particle takes to first move a distance r from its initial position. As discussed by Hurley and Harrowell [15], the proper choice of r is crucial in resolving the intermediate-time kinetic heterogeneities in the liquid. If the length r is too short, then the oscillatory motion of the particles at their local positions cannot be distinguished from diffusive motion. As a result, the spatial distribution of the local relaxation times will be random. This is shown in figure 2 for $r = 0.1$ for the equimolar binary mixture at $T^* = 1$ and 0.4. Here the fast and slow particles are randomly distributed throughout the simulation cell (compare with figure 3) and one cannot differentiate between the high- and low-temperature systems by just looking at these spatial relaxation time maps.

At the other extreme, if the distance r is too long, there will also be little correlated structure in the relaxation time maps, since particles would have sampled several fast and slow domains before exceeding this distance. Thus, the degree of spatial segregation of the kinetic inhomogeneities in sufficiently dense systems is expected to pass through a maximum as r is increased from zero. For the binary mixture this maximum, as shall be described later below, occurs when $r \approx 1.0$. Examples of what the kinetic structure looks like for $r = 1$ are shown in figure 3 for $T^* = 1$, 0.6, 0.5 and 0.4. Here the fastest 40%

and the slowest 40% of particles at their initial positions for a given run are shown by the open and filled circles respectively. Although the distribution of relaxation times is mapped over the *initial* positions of the particles, a similar amount of correlated structure at a given temperature and the trends observed in figure 3 as the system is cooled are also obtained if the *final* positions of the particles are used instead, since the particles have not moved very far from their initial positions by the time the first 60% of the particles have first moved a distance of σ_1. At $T^* = 1$, for example, the average MSD for this batch of fastest particles at this time is less than $1.5\sigma_1^2$.

From figure 3 a clear clustering of particles into domains of similar mobility can be seen as the system is cooled. In other words, the probability of a particle being slow if it is initially surrounded by other slow particles, or being fast if it is originally in the midst of fast neighbours, increases significantly as the temperature drops. Note that although the relaxation time maps in these figures are for the same cut-off distance r, the average time taken for all of the particles to first move the length r increases very rapidly with decreasing temperature. In fact, for a given run at $T^* = 0.4$, the few slowest particles in the system have not moved the distance of σ_1 even by $t = 15\,000\,\tau$ which is greater than the time taken for the incoherent scattering functions at this temperature to decay to zero as shown in figure 1. We find that for $r > 0.5\sigma_1$, the time required for the slowest 5% of particles at $T^* = 0.4$ to first move the distance r becomes too long and impracticable to simulate. We can still, however, plot the spatial distribution of fractions of fast and slow particles at $T^* = 0.4$ as shown in figure 3(d), since once the relaxation times of the required number of 40% fast and 20% intermediate particles are known, the rest of the particles can be designated as slow without having to determine their relaxation times explicitly.

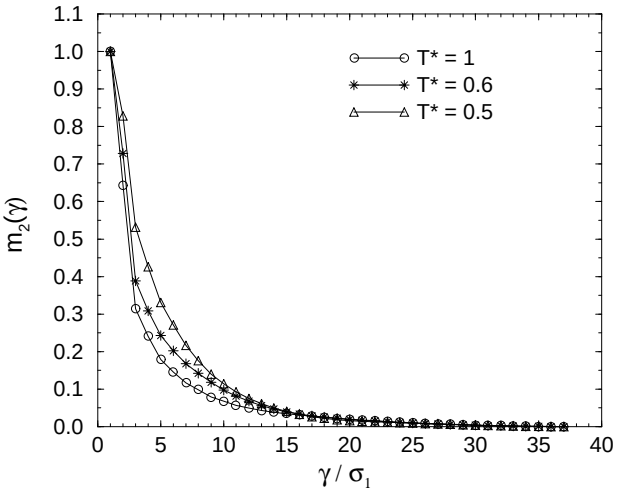

Figure 4. The decay of the second moment $m_2(\gamma)$ as defined in equation (3) for $T^* = 1$, 0.6 and 0.5. These curves are from the individual runs which gave rise to the relaxation time maps of the corresponding temperatures shown in figure 3.

3.2. Quantifying the kinetic structure

In order to quantify the variation of the kinetic structure with r, as well as to measure the increase in the size of the fast and slow domains with decreasing temperature, we perform

the coarse-graining procedure of Hurley and Harrowell [15] and assign to each particle i the mean local relaxation time $\tau_{i,\gamma}$ of a subcell of dimension $\gamma \times \gamma$ centred at the initial position of particle i. The idea is that as γ is varied from 1 to the length of the simulation box L, the local relaxation time $\tau_r(i) = \tau_{i,1}$ of particle i is expected to become uncorrelated with the mean relaxation time $\tau_{i,\gamma}$. This is indicated by the decay of the second moment $m_2(\gamma)$ of $\tau_{i,\gamma}$ defined as

$$m_2(\gamma) = \frac{\langle(\tau_{i,\gamma} - \tau_{i,L})^2\rangle}{\langle(\tau_{i,1} - \tau_{i,L})^2\rangle} \qquad \gamma \in [1, L] \tag{3}$$

where $\tau_{i,L}$ is the local relaxation time averaged over all the particles for a particular run, and the angular brackets denote an average over subcells indexed by i and over different configurations. An example of the decay of $m_2(\gamma)$ with γ is shown in figure 4 for the binary mixture at $T^* = 1$, 0.6 and 0.5 for a cut-off distance of $r = 1$.

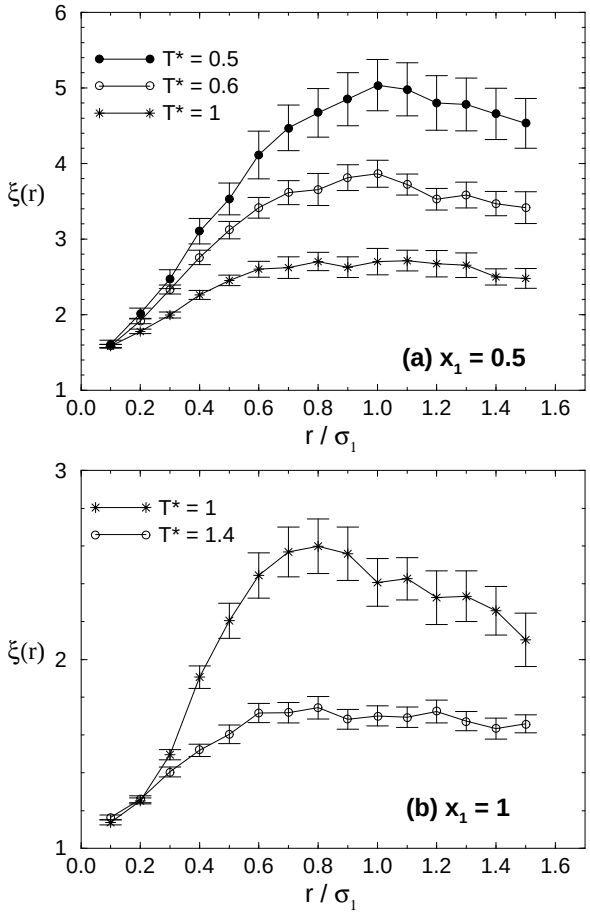

Figure 5. The variation of the kinetic correlation length $\xi(r)$, defined in equation (4), with the cut-off distance r for (a) the equimolar binary mixture at $T^* = 0.5$, 0.6 and 1, and for (b) the single-component system of small particles at $T^* = 1$ and 1.4. The error bars are twice the standard deviations about the average data points.

A measure of the spatial correlations in the particle dynamics for a particular value of r is provided by the area under $m_2(\gamma)$:

$$\xi(r) = \int_1^L m_2(\gamma)\ \mathrm{d}\gamma. \tag{4}$$

A plot of this characteristic length $\xi(r)$ versus r is given in figure 5(a) for the equimolar binary mixture at $T^* = 1$, 0.6 and 0.5. Between 20 to 100 runs were averaged over to obtain ξ for each value of r. There are several features to notice.

(i) At $r = 0.1$, the correlation length ξ is the same for high and low temperatures, consistent with the random configurations at $T^* = 1$ and 0.4 shown in figure 2 for this cut-off distance.

(ii) As r is increased, $\xi(r)$ goes through a broad maximum with an approximately temperature-independent peak at about $r = 1.0$.

(iii) The height of this peak increases with decreasing temperature, again consistent with the greater degree of clustering observed in figures 3(a) to 3(d) as the temperature is lowered.

(iv) The maximum kinetic length at the peak is significantly longer than that associated with random clustering at very small r.

For comparison, the variation of the correlation length for the single-component system of small particles is shown in figure 5(b) for $T^* = 1$ and 1.4. Here the maximum in $\xi(r)$ occurs at $r \approx 0.8$ in agreement with the temperature-independent value obtained by Hurley and Harrowell in their constant-NVE simulations. In the case of the pure liquid, the increase in the height of the peak in $\xi(r)$ is due to the formation of transient hexagonal clusters that increase in size as the temperature is lowered. Eventually one of these crystalline nuclei is able to span the entire system at the freezing transition, $T^*_{f,1} = 0.95$, at which time ξ diverges for all but the smallest values of r. For the binary mixture, the increase in the magnitude of the maximum correlation length with decreasing temperature is not due to any phase separation and crystallization into ordered phases, but is instead brought about by an increase in the degree of cooperative motion in the mixture.

The development of spatially heterogeneous dynamics in the 2D mixture is accompanied by a slowing down of the system. In figure 6 we plot the temperature dependence of the average local relaxation time $\tau_{\mathrm{av}} = \langle \tau_{i,L} \rangle$ for $r = 1$ in an Arrhenius plot. From now on, the analysis is restricted to the case of $r = 1$, where the resolution of the kinetic structure is maximized. The same conclusions will be reached using other values of r around the peak maximum in $\xi(r)$. As can be seen, τ_{av} has an Arrhenius temperature dependence down to $T^* = 0.55$. Below this temperature, the average relaxation time diverges from Arrhenius behaviour. We were unable to determine τ_{av} at $T^* = 0.4$, since this requires the relaxation of all particles and for this temperature, as mentioned above, the time required for the very slowest particles to first move a distance $r = 1$ is too long for us to simulate. Structural relaxation times determined from the decay of incoherent and coherent intermediate scattering functions to 1/e of their initial values also display an Arrhenius temperature dependence for $T^* \geqslant 0.55$, albeit with different activation energies, and a departure from such high-temperature behaviour at $T^* < 0.55$ [10, 11, 12, 14].

In figure 6 we also show the temperature variation of a measure of the average width of the distribution of local relaxation times $\tau_r(i)$ about τ_{av} for $r = 1$, defined as

$$\chi = \left\langle \sqrt{\frac{1}{N-1} \sum_{i=1}^{N} (\tau_{r=1}(i) - \tau_{\mathrm{av}})^2} \right\rangle \tag{5}$$

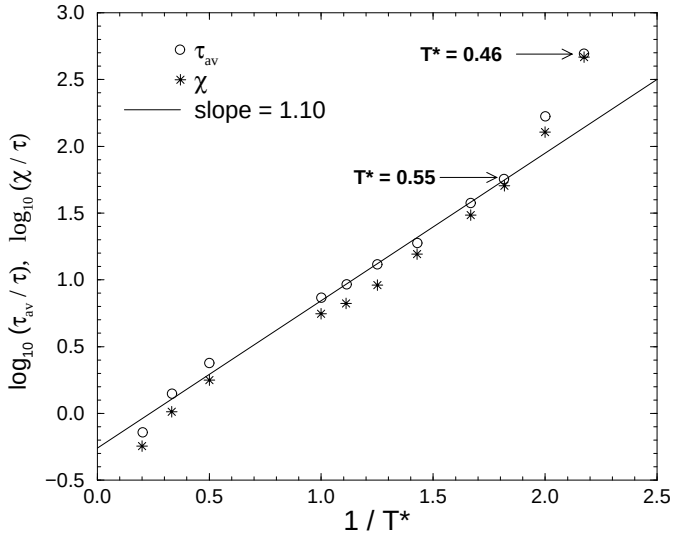

Figure 6. An Arrhenius plot of the temperature dependence of (i) the average local relaxation time τ_{av} and (ii) the average standard deviation χ of the distribution of local relaxation times about the mean for a cut-off distance of $r = \sigma_1$. The solid line is a linear regression through $\log_{10}\tau_{\mathrm{av}}$ for the temperature range $T^* \in [0.55, 5]$. It has a slope of $1.10\epsilon/k_B$.

where the angular brackets denote an average over different runs. As can be seen in figure 6, this average standard deviation χ follows the temperature dependence of τ_{av} and is greater than $0.7\tau_{\mathrm{av}}$ for $T^* \in [0.46, 5]$, reaching $0.93\tau_{\mathrm{av}}$ at $T^* = 0.46$. It is clear from the plot that the width of the distribution of relaxation times broadens considerably as the temperature is lowered.

3.3. Variation of the average relaxation time with the kinetic length scale

An interesting relationship is found between the average relaxation time τ_{av} and the kinetic correlation length $\xi(r = 1)$ in the moderately supercooled region. In figure 7 a plot of $\log_{10}\tau_{\mathrm{av}}$ against $\log_{10}\xi(r = 1)$ is shown. It is found that in the range $T^* \in [0.5, 1]$, $\tau_{\mathrm{av}} \propto \xi^{4.3}$, which indicates how small increments in ξ are magnified to much larger increases in τ_{av}. The power law breaks down below $T^* = 0.5$ where the temperature dependences of the structural relaxation times from the intermediate scattering functions and τ_{av} are observed to diverge from the high-temperature Arrhenius behaviour. Thus in the deeply supercooled region, there is a dramatic slowing down with falling temperature which is accompanied by only a very small increase in ξ.

A power-law dependence similar to that described above was obtained by Yamamoto and Onuki [6, 7] for the same system, but for different definitions of relaxation time and kinetic correlation length. They studied the dynamics of this 2D mixture under varying rates of shear using MD simulations. In their analysis, pairs of particles were considered to be 'bonded' if at an initial time, the separation between them $r_{ij} \leqslant 1.1\sigma_{ab}$. At some later time, a bond is defined to be broken if $r_{ij} > 1.6\sigma_{ab}$. By monitoring the distribution of broken bonds, Yamamoto and Onuki observed that bond breakage became increasingly spatially heterogeneous with decreasing temperature for a particular shear rate, and with decreasing shear rate for a particular temperature. They defined a relaxation time τ_b for a given temperature and shear rate to be the time at which 5% of initial bonds are broken

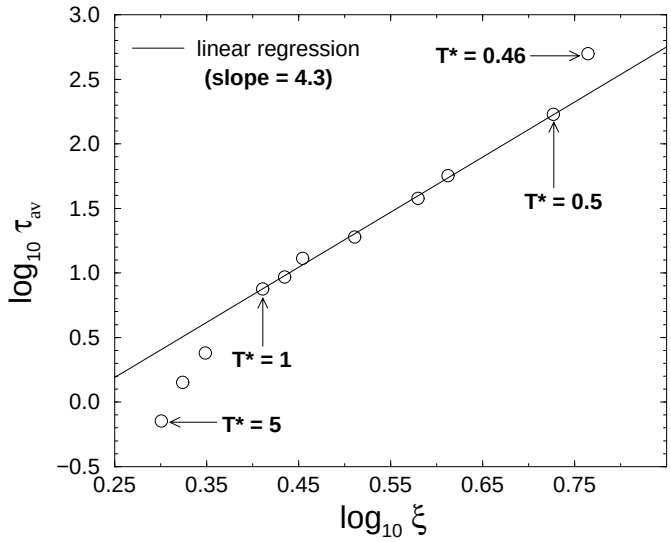

Figure 7. The variation of $\log_{10}\tau_{\rm av}$ with $\log_{10}\xi(r=1)$ for the 2D binary mixture. The solid line is a linear regression through the points for the temperature range $T^* \in [0.5, 1]$. It has a slope of 4.3 which indicates that $\tau_{\rm av} \propto \xi^{4.3}$ in this temperature interval.

in a time interval of $0.05\tau_b$. From the structure factor of the broken bond density, they estimated the characteristic size ξ_b of the clusters of broken bonds and obtained $\tau_b \propto \xi_b^4$ for all temperatures and shear rates used in their simulations. The temperature range that they investigated was $T^* \in [0.337, 2.54]$.

To arrive at a similar scaling exponent from such different definitions of the kinetic length scale suggests that the exponent of approximately 4 may be a robust feature of this simple 2D mixture, at least over an intermediate range of timescales. It would be interesting to investigate whether the power law with the same exponent holds for other diameter ratios for which the 2D mixture can be quenched into amorphous states without crystallization. Foley and Harrowell [18] have carried out the same analysis as we have done above for the 2D facilitated kinetic Ising spin model [19] and obtained $\tau_{\rm av} \propto \xi^{12.6}$. This much larger exponent is most probably due to the higher degree of cooperativity that is built into this system as a result of the specific dynamical correlations between spins that are explicitly specified at the outset. Yamamoto and Onuki [7] have also performed their same bond breakage analysis on a 3D equimolar binary mixture with $\sigma_2/\sigma_1 = 1.2$. This time they obtained $\tau_b \propto \xi_b^2$ for all temperatures and shear rates in their simulations. The smaller exponent in 3D indicates that a greater degree of spatial correlation in particle kinetics is required to 'jam' particle motion in 3D than in 2D, due to the additional degree of spatial freedom in 3D. It would also be interesting to examine whether the power law with an exponent of 2 is a general characteristic of systems of spherical particles in 3D.

4. Fast and slow contributions to self-diffusion

Once the distribution of local relaxation times at a particular temperature is known, particles can be assigned arbitrarily into fast and slow subsets, and the contribution of each subgroup

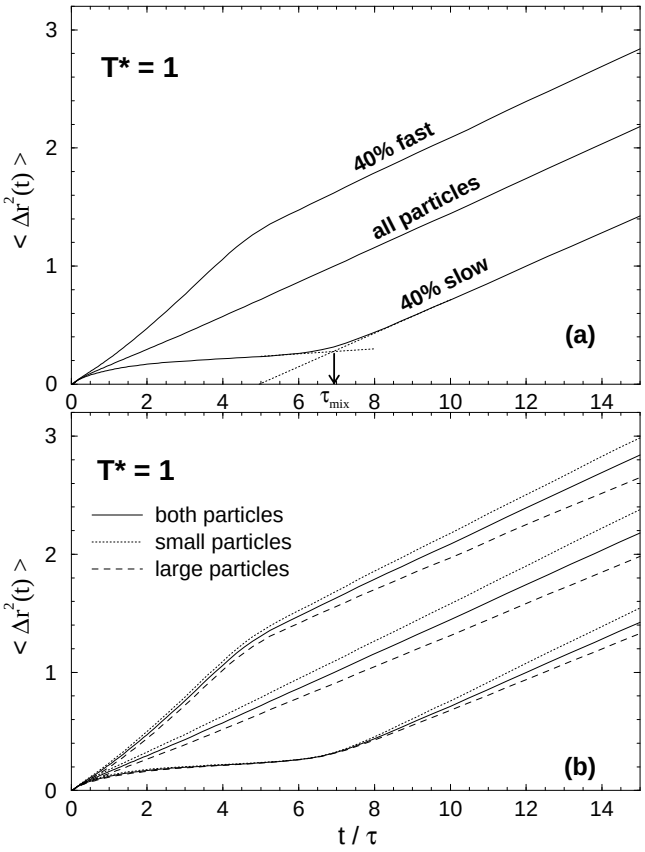

Figure 8. (a) The mean squared displacement (MSD) for the binary mixture at $T^* = 1$ and the contributions to this average curve from the slowest 40% and the fastest 40% of particles in the system for the cut-off distance $r = \sigma_1$. The mixing time τ_{mix} of the slow particles is defined as the intersection of the extrapolated plateau height and the long-time linear behaviour as shown by the dotted lines. (b) The solid lines are as in (a) above, and the dotted and dashed lines are the contributions to each of these curves from the small and large particles respectively.

to time-dependent properties can be determined. In figure 8(a) we show the average MSD

$$\left\langle \Delta r^2(t) \right\rangle = (1/N) \left\langle \sum_{i=1}^{N} [r_i(t) - r_i(0)]^2 \right\rangle$$

for all of the particles in the binary mixture at $T^* = 1$, as well as the contributions to this average from the fastest 40% and the slowest 40% of particles, irrespective of particle type. Although this fractioning is crude, it does serve to provide some important insights into the dynamics of various subpopulations of particles.

At this junction, before describing the results shown in figure 8, a brief discussion is required to explain the observed linear dependence of the MSD shown in figure 8 (and also in figures 9 and 11—see later) at long times. In 1970, Alder and Wainwright [20] demonstrated that persistent hydrodynamic flows were established around circular particles in very low density 2D liquids. This 'backflow' results in a velocity autocorrelation function which decays as t^{-1} and a MSD which grows faster than linearly with time. The self-diffusion

coefficient defined equivalently as

$$D = \frac{1}{4} \lim_{t\to\infty} \mathrm{d}\left\langle \Delta r^2(t) \right\rangle / \mathrm{d}t$$

or

$$D = \frac{1}{2} \int_0^\infty \langle \boldsymbol{v}(0) \cdot \boldsymbol{v}(t) \rangle \ \mathrm{d}t$$

where $\boldsymbol{v}(t)$ is the velocity vector of a particle at time t, must diverge under such circumstances. In contrast to these results which have concentrated on *low* density calculations, it was shown by Hurley and Harrowell [21] that for a single-component system of soft discs near the freezing temperature, there is no long-time tail in the velocity autocorrelation function and the MSD increases linearly with time in the diffusive regime. We have also previously shown [22] that supercooled mixtures of soft discs with varying diameter ratios exhibit similar long-time linear diffusive behaviour. At these low temperatures and high densities, transient crystalline fluctuations are observed in the 2D liquids. Spatial maps of velocity correlations, similar to those in reference [20], indicate local elastic behaviour rather than hydrodynamic flow [23]. These features lead us to suggest that propagating transverse modes become of increasing importance in transporting away the local shear momentum as the density increases. This mechanism would diminish the amplitude of any residual viscoelastic flow and, presumably, account for the absence of the anomalous diffusive behaviour observed at much lower densities.

Returning to figure 8(a), although on intermediate timescales the average MSD over all of the particles has already reached its long-time linear behaviour, a substantial fraction of the system is still 'caged' as indicated by the plateau in the MSD of the slowest 40% of particles. The lifetime of this slow cage is given by the mixing time τ_{mix}, which we define graphically in figure 8(a) as the time corresponding to the intersection of the extrapolated plateau height and the extrapolated linear region beyond the plateau. Even in the fluid mixture at $T^* = 1$, this mixing time is already approximately 690 average collision times t_c. (For $T^* \leqslant 3$, $t_c = 0.11 \pm 0.01\tau$ and is only very weakly dependent on temperature.) Beyond τ_{mix}, the slow particles have sampled faster domains and lost the memory of their initial kinetic state. Hence the MSD of this slow fraction at $t > \tau_{\mathrm{mix}}$ has the same slope as the total average. Similarly, the fastest 40% of particles retain their identity over many collision times, as shown by the enhanced diffusion in figure 8(a), until mixing with slower particles eventually results in a turnover of the MSD of this subgroup to the same slope as for the average MSD over all of the particles. The mixing time of the fast particles is shorter than that of the slower particles, since they are able to translate over longer distances while the slow particles are caged. The stability of the kinetic structure that is defined by the arbitrary partitioning of particles into 40% fast and 40% slow groups is determined by the mixing time of the slow particles.

In figure 8(b), we show the contribution from the small and large particles respectively to each of the MSD curves shown in figure 8(a). Observe that on the timescale over which the slowest 40% of all the particles are caged, *both* the small and large particles in this fraction are trapped. Only at $t \approx \tau_{\mathrm{mix}}$ do the mean squared displacements of both of these components diverge from one another to acquire the same slope as the MSD averaged over all of the particles of the respective species. Similarly, each of the contributions from the small and large particles in the fastest 40% subset rolls over to the same diffusion constant as the global average over the corresponding species after the mixing time of this fast group. In the diffusive region, it is not surprising that the diffusion constant of the small particles is greater than that of the large particles given that the masses of both types of particle are equal.

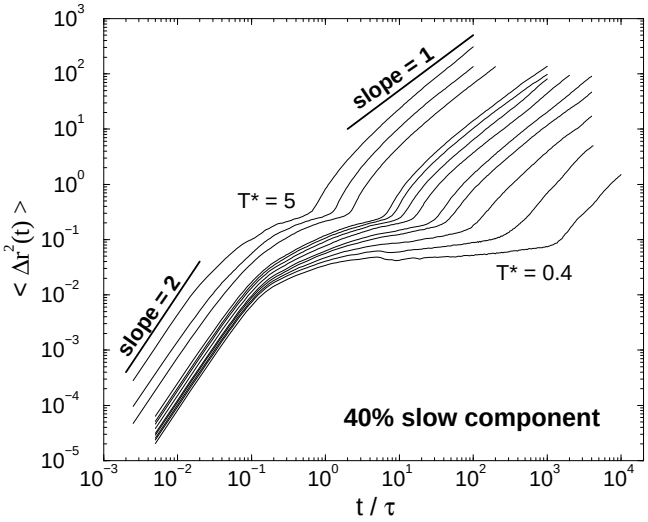

Figure 9. A log–log plot of the mean squared displacement against time at various temperatures for the slowest 40% of particles in the binary mixture for $r = \sigma_1$. From left to right the curves correspond to $T^* = 5$, 3, 2, 1, 0.9, 0.8, 0.7, 0.6, 0.55, 0.5, 0.46 and 0.4.

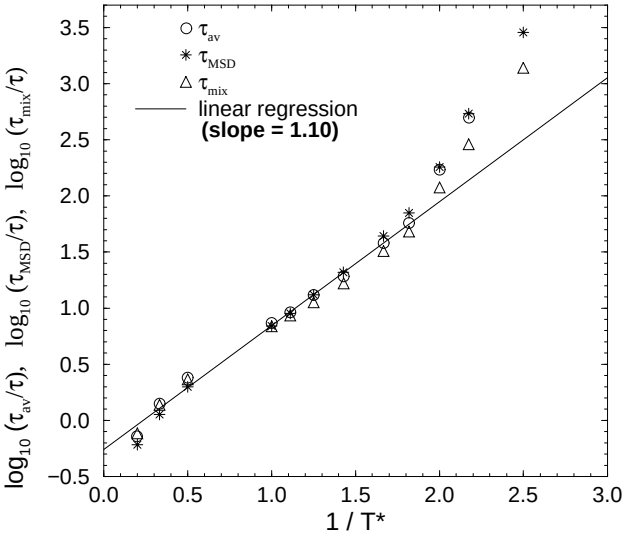

Figure 10. An Arrhenius plot of $\tau_{\rm av}$, $\tau_{\rm MSD}$ and $\tau_{\rm mix}$ as defined in the text. The solid line is a linear regression through the points for $\tau_{\rm av}$ in the range $T^* \in [0.55, 5]$.

The height of the plateau in the MSD of the slowest 40% of particles decreases slightly with falling temperature. This is shown in figure 9 where the MSD of this slow fraction is plotted against time in a log–log plot for a range of temperatures from $T^* = 5$ to 0.4. At very short times, these slow particles undergo ballistic motion. The MSD then curves over to a very small slope, indicating the trapping of the particles in the cage of their neighbours. This plateau ends at $\tau_{\rm mix}$ where there is a rapid upturn in the MSD which eventually leads to diffusive motion. The lifetime of the transient cage increases significantly with decreasing

temperature until it extends over more than three decades at $T^* = 0.4$.

The temperature dependence of τ_{mix} is displayed in figure 10 in an Arrhenius plot. Also shown for comparison is the temperature dependence of τ_{av} and τ_{MSD}, which is the time for which the MSD averaged over all of the particles is equal to 1. τ_{av} and τ_{MSD} coincide within statistical error which indicates that the average time taken by the particles to *first* move a distance of σ_1 is approximately the same as the time corresponding to an average displacement of σ_1. The mixing time τ_{mix} coincides with τ_{av} at higher temperatures, but becomes slightly less than τ_{av} at lower temperatures, with the difference between these two times increasing in the non-Arrhenius region below $T^* = 0.55$.

Despite the persistence of the transient slow domains over many collision times as measured by τ_{mix}, a substantial amount of structural relaxation can still be accomplished. This can be seen, for example, by noting the amount of decay in $F_{s,1}(k_1, t)$ and $F_{s,2}(k_2, t)$, shown in figure 1, at τ_{mix}. More than 80% of the relaxation functions have decayed by the time τ_{mix} is reached for $T^* \geqslant 0.4$ for $F_{s,1}(k_1, t)$ and for $T^* \geqslant 0.5$ for $F_{s,2}(k_2, t)$. At the higher temperatures, even more than 90% relaxation can be accomplished before τ_{mix}. For the incoherent scattering function of the larger particles which decays more slowly than that of the small particles, at least 60% decay can still occur by τ_{mix} in the deeply supercooled liquid at $T^* = 0.46$ and 0.4. These results imply that a significant amount of relaxation, as measured by the incoherent scattering functions, can be accomplished by the enhanced diffusion of the more mobile particles in the mixture before τ_{mix} (see figure (8a)), as well as by correlated, small-amplitude, anharmonic fluctuations of the caged slow domains. *These results highlight an important point that, even though a particular relaxation function has decayed substantially, there may still be significantly large regions in the system that are relatively immobile and have not yet randomized their initially slow kinetic state.*

The results in the previous paragraphs have focused on the crude partitioning of particles

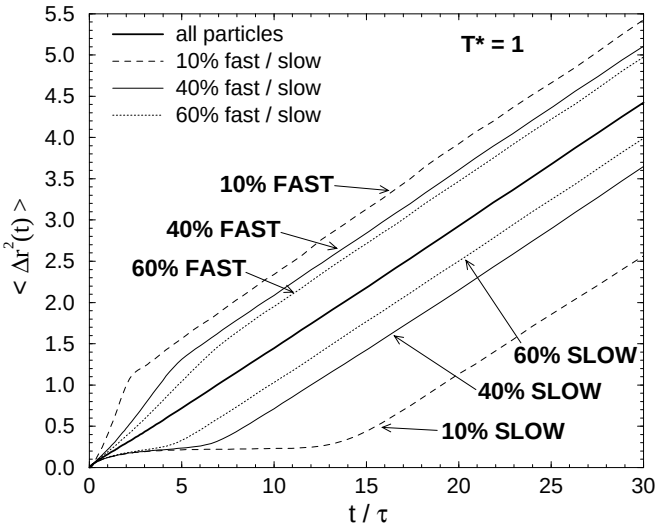

Figure 11. The MSD averaged over all of the particles at $T^* = 1$ for the binary mixture is shown by the thick solid line in the centre. The contributions to this curve from the fastest 10%, 40% and 60% of particles are shown by the dashed, solid and dotted lines respectively lying above it. Similarly, the contributions to the average MSD from the slowest 10%, 40% and 60% of particles are given by the dashed, solid and dotted lines lying below the thick solid line. The fractions of fast and slow particles were determined using the cut-off distance $r = \sigma_1$.

into the fastest 40% and the slowest 40%. This division, as stated earlier, is arbitrary. In figure 11 we show the contributions to the MSD at $T^* = 1$ from the slowest and fastest groups composed of three different numbers of particles. As can be seen, the mixing time of the slowest subset of particles increases as the fraction of this group decreases, since the more mobile particles are being sieved out and only the very slowest particles are being left behind. For the slowest 10% of the particles, more than 95% of $F_{s,1}(k_1, t)$ and $F_{s,2}(k_2, t)$ have decayed at this temperature while these particles are still caged, which again emphasizes the fact that slower relaxational processes can still exist in the system despite the nearly complete relaxation displayed by a specific relaxation function. For the fast particles, as the size of this subpopulation is increased, the contribution to the MSD approaches that of the total average and the mixing time increases, since more and more slow particles are being added to this subgroup. This also explains why the diffusion constant of the enhanced motion before mixing decreases as the fraction of fast particles is increased.

5. Visualization of relaxation kinetics

A picture of the temporal sequence of the process of relaxation in the 2D mixture can be obtained by viewing individual spatial maps of the kinetic domains in order of the fastest to slowest particles as described in the following. In figure 12 and continued in figure 13 we show a series of snapshots of the initial positions of an incrementally increasing fraction of the fastest particles (determined using $r = 1$) for a run at $T^* = 1$ and 0.4 for the binary mixture. These are the same runs as were used to generate the configurations in figures 3(a) and 3(d) for these temperatures. Figure 12 shows that for $T^* = 1$, the first 10% of the fastest particles are randomly distributed throughout the system with very little clustering. This allows for almost simultaneous relaxation in widely separated and disconnected regions. The next 10% of the fastest particles emerge close to pre-existing fast sites, as well as appearing spontaneously in slow domains. This trend continues as relaxation progresses. At $T^* = 0.4$, a distinct difference in the sequence of relaxation can clearly be seen. The majority of the first 10% of the fastest particles are clumped together rather than being widely spaced out throughout the system. Relaxation then proceeds by spreading outwards from these fast centres by the formation of string-like correlations of fast particles to link up disconnected domains of fast particles. Fewer new relaxing centres appear spontaneously in slow regions compared to the case for $T^* = 1$ and there is less mixing between fast and slow particles, resulting in large compartmentalized blocks of diverse kinetics at $T^* = 0.4$ (compare the 60% configurations at $T^* = 1$ and 0.4 in figure 13).

The main difference between the spatial advancement of relaxation at the high and low temperatures is that, because at the higher temperature, the first few fastest particles are randomly distributed; the spreading of relaxation outwards from these fast relaxing sites gives rise to a more spatially homogeneous distribution of relaxation. On the other hand, because at the lower temperature, the initial fast particles tend to be clustered together; this leads to a less uniform progression of relaxation throughout the system. The picture of relaxation propagating outwards from fast relaxing sites is consistent with the general idea of relaxation mediated by diffusing defects [24, 25].

The correlated string-like motion at the lower temperature involving a significant number of particles over timescales more than four orders of magnitude longer than the average collision time can also be observed in particle trajectory plots [10, 12, 14]. A detailed analysis of the particle trajectories is provided in reference [14].

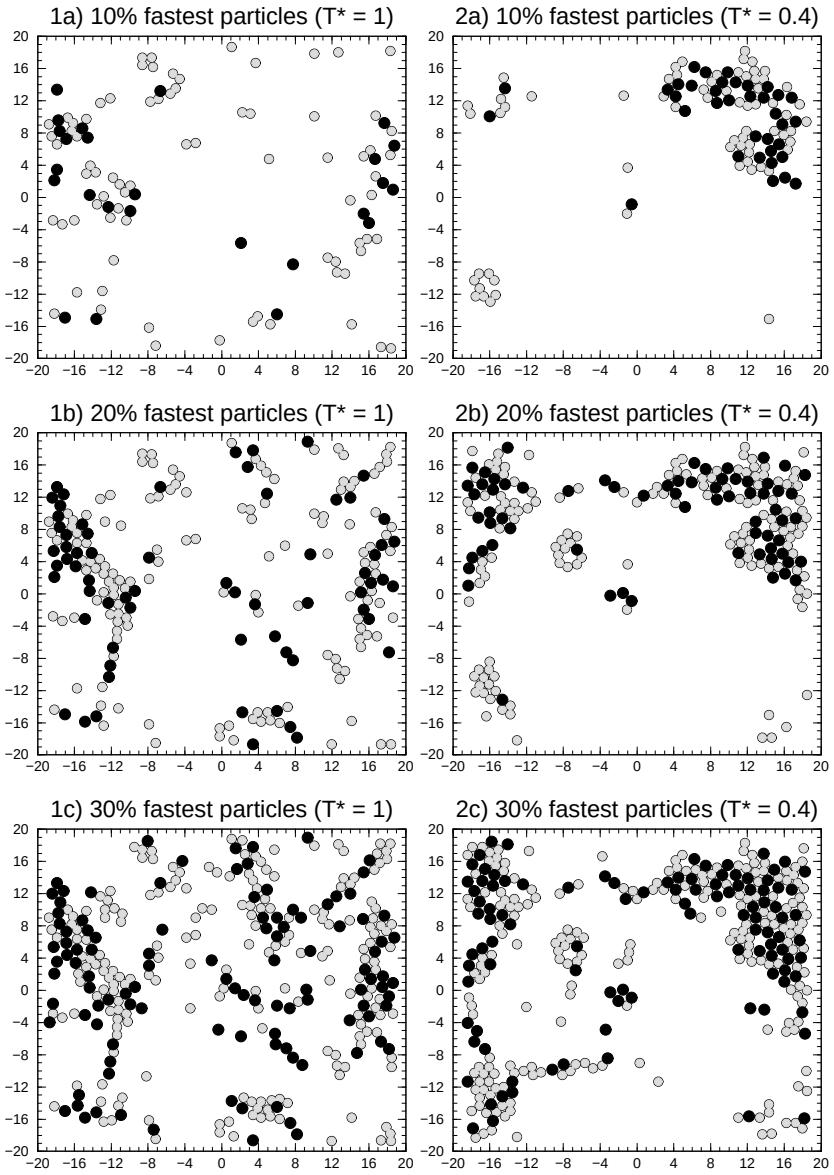

Figure 12. The initial positions of the fastest 10%, 20% and 30% of particles determined using $r = 1$ for single runs at $T^* = 1$ (on the left) and $T^* = 0.4$ (on the right). The small and large particles are shown by the grey and black circles respectively. The particles are not drawn to scale. Observe the random distribution of the first few fastest particles at $T^* = 1$, and the clustering of these particles at $T^* = 0.4$.

6. Summary and conclusions

In summary, we have presented a quantitative analysis of the development of spatially heterogeneous dynamics in a simple model fragile glass-former consisting of an equimolar binary mixture of soft discs. By defining a local relaxation time in terms of the time taken to first move a distance r from a starting position, the underlying kinetic structure at varying

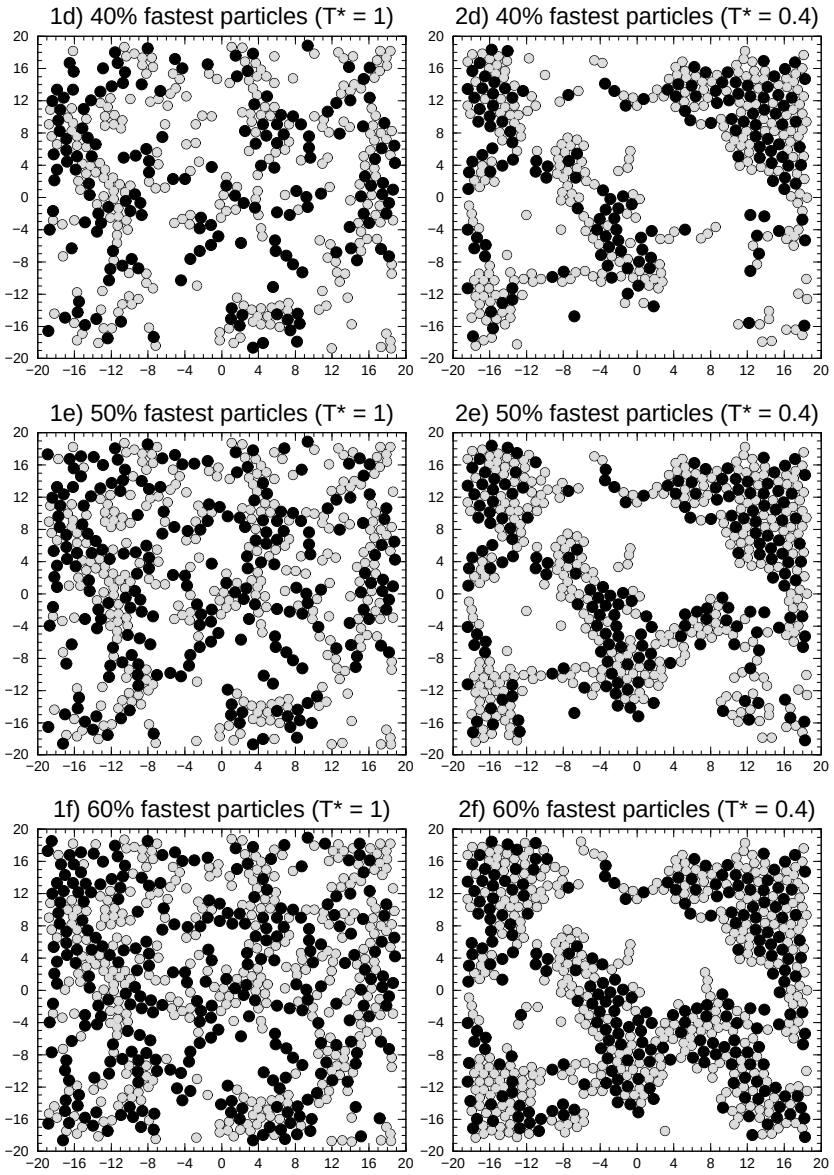

Figure 13. A continuation of figure 12 showing the initial positions of the fastest 40%, 50% and 60% of particles for $T^* = 1$ (left) and $T^* = 0.4$ (right). These runs were used to generate the relaxation time maps shown in figures 3(a) and 3(d) for these temperatures. In fact, the 60% configurations shown here are the same as the spatial maps shown in figure 3 for $T^* = 1$ and 0.4 with the white regions in these configurations corresponding to the slow black domains in figures 3(a) and 3(d).

length scales can be resolved. It is found that a distance of approximately one small particle diameter is sufficient to maximize the segmentation of the particle dynamics into domains of correlated kinetics that increase in size as the temperature drops. A kinetic correlation length ξ was defined as a measure of the size of these clusters, and in the moderately supercooled region down to $T^* = 0.5$, the average time taken to first travel a length $r = \sigma_1$ was found

to vary as $\tau_{av} \propto \xi^{4.3}$. Below this temperature the power law breaks down as τ_{av} and other structural relaxation times begin to increase much more rapidly than predicted by their higher-temperature Arrhenius behaviour. Thus, in the deeply supercooled mixture, only a very small increase in this correlation length accompanies the dramatic rise in relaxation times, which suggests that ξ does not diverge below T_g. The power law with the same exponent of 4 has been found in previous and different kinetic studies of this 2D mixture by Yamamoto and Onuki [6, 7] which suggests that this exponent may be characteristic of this particular system. They also obtain a smaller exponent of 2 for a 3D binary mixture.

From the distribution of local relaxation times, the contributions to time-dependent correlation functions from varying fractions of the fastest and slowest particles in the system can be determined. By analysing the contributions to the MSD from kinetically disparate groups of particles, it is found that only subsets of the slowest particles are caged on intermediate timescales. Even for a large fraction of 40% of the slowest particles, the lifetime of the cage in the fluid mixture at $T^* = 1$ extends over more than two orders of magnitude longer than the average collision time t_c. The mixing time of these slowest 40% of particles, which is the time required for this subgroup to lose the memory of its initial kinetic state, increases with decreasing temperature, until in the deeply supercooled mixture at $T^* = 0.4$, it is more than four orders of magnitude longer than t_c. Both the small and large particles in the slow subset are equally trapped during the lifetime of the transient cage.

A substantial amount of initial decay in the incoherent scattering functions (more than 80% except at the very lowest temperatures) is observed to occur while a large fraction (40%) of the system is still trapped in the transient cages. This indicates that a significant amount of initial relaxation in the scattering functions is accomplished by the enhanced diffusion of the fast particles that occurs before their mixing time, as well as by the small-amplitude anharmonic oscillations of the slow particles in their cages. This result emphasizes the point that even slower relaxational processes may still be prevalent despite the nearly complete decay of a specific relaxation function.

The spatial development of relaxation as a function of temperature was also investigated by plotting the positions of the particles in order of the fastest to the slowest. It is found that at the higher temperatures, the first few fastest particles are randomly distributed in the system, but at lower temperatures they tend to form large clusters. At both high and low temperatures, relaxation proceeds primarily by spreading outwards from existing fast sites, with a tendency to form 'bridges' of string-like correlations of particles to link up fast domains that are initially separated from one another. Due to the initially less homogeneous distribution of the fast particles at the lower temperatures, this mechanism of relaxation results in a spatial fragmentation of the system into large blocks of slow and fast kinetics in the deeply supercooled mixture.

In conclusion, the emergence of a slower relaxational process with decreasing temperature in the 2D binary mixture is shown to be intricately coupled to the onset of an increasing degree of dynamic heterogeneity in the system, which is induced by the growing degree of cooperativity in particle dynamics with increasing density. This heterogeneity is characterized by both a broadening of the distribution of local relaxation times and an increasingly coarser distribution in space of these times with supercooling. This work has provided a quantitative and visual analysis of the development of these spatial diversities in local kinetics. The methodology can easily be extended to 3D. Recently, Perera and Harrowell [11] have presented another method of detecting dynamic heterogeneity without the need to resort to an explicit resolution of the spatial distribution of local mobilities. They have also shown how the growing degree of dynamic heterogeneity is responsible in part

for the different temperature dependences of structural relaxation and self-diffusion [11].

As mentioned in the introduction, there is growing evidence from real experiments and computer simulations of the existence of kinetic inhomogeneities in many other supercooled fragile glass-formers. This leads to an inevitable question of whether the development of slow (or glassy) relaxation with supercooling is inseparable from that of spatially heterogeneous dynamics in fragile liquids. It seems plausible that this is indeed a general feature of fragile liquids. As the liquid is cooled below its freezing temperature, there is always an increasing thermodynamic driving force which will favour local ordering. Regions which do not lie close to structural defects will become increasingly more ordered as the temperature drops. These locally ordered domains are expected to become the slowest relaxing regions in the system. As the size and lifetime of these slow ordered clusters increase, so too does the degree of dynamic heterogeneity and slow relaxation increase in the system. For strong liquids, which have a three-dimensional, tetrahedral or other network pervading the system, the local ordering which arises from the loss of thermal energy is expected to be homogeneously distributed throughout the system. Thus, these systems are expected to slow down continuously with decreasing temperature without any dramatic changes in dynamics. In order to test this prediction, more experiments to probe transient kinetic inhomogeneities need to be conducted on both fragile and strong liquids alike. The author is unaware of any such experiments being carried out on supercooled strong liquids. Direct observation of the *size* and *spatial* distribution of local kinetic domains in real systems also remains a formidable experimental challenge.

Acknowledgments

I am grateful for the receipt of an STA Post-Doctoral Fellowship from the Japanese Government. I would also like to thank Dr Peter Harrowell for many stimulating and encouraging discussions.

References

[1] Schmidt-Rohr K and Spiess H W 1991 *Phys. Rev. Lett.* **66** 3020
Leisen J, Schmidt-Rohr K and Spiess H W 1993 *Physica* A **201** 79
Heuer A, Wilhelm M, Zimmermann H and Spiess H W 1995 *Phys. Rev. Lett.* **75** 2851

[2] Ehlich D and Sillescu H 1990 *Macromolecules* **23** 1600
Fujara F, Geil B, Sillescu H and Fleischer G 1992 *Z. Phys.* B **88** 195
Chang I, Fujara F, Geil B, Heuberger G, Mangel T and Sillescu H 1994 *J. Non-Cryst. Solids* **172–174** 248

[3] Cicerone M T and Ediger M D 1995 *J. Chem. Phys.* **102** 471
Cicerone M T and Ediger M D 1995 *J. Chem. Phys.* **103** 5684
Cicerone M T and Ediger M D 1996 *J. Chem. Phys.* **104** 7210

[4] Blackburn F R, Cicerone M T and Ediger M D 1994 *J. Polym. Sci., Polym. Phys. Edn* **32** 2595
Blackburn F R, Cicerone M T, Hietpas G, Wagner P A and Ediger M D 1994 *J. Non-Cryst. Solids* **172–174** 256
Cicerone M T, Blackburn F R and Ediger M D 1995 *Macromolecules* **28** 8224

[5] Muranaka T and Hiwatari Y 1995 *Phys. Rev.* E **51** R2735

[6] Yamamoto R and Onuki A 1997 *Europhys. Lett.* **40** 61
Yamamoto R and Onuki A 1997 *J. Phys. Soc. Japan* **66** 2545

[7] Yamamoto R and Onuki A 1998 Nonlinear rheology of highly supercooled liquids *Proc. 2nd Tohwa University Int. Mtg on Statistical Physics (Fukuoka, Japan, 1997); J. Non-Cryst. Solids* at press

[8] Donati C, Douglas J F, Kob W, Plimpton S J, Poole P and Glotzer S C 1998 *Phys. Rev. Lett.* **80** 2338
Web site at http://www.ctcms.nist.gov/ donati/

[9] Perera D N and Harrowell P 1998 Dynamical correlations in a two dimensional binary mixture *Proc. 2nd Tohwa University Int. Mtg on Statistical Physics (Fukuoka, Japan, 1997); J. Non-Cryst. Solids* at press

[10] Perera D N and Harrowell P 1998 Resolving the collective relaxation dynamics in a supercooled binary mixture *Proc. 2nd Tohwa University Int. Mtg on Statistical Physics (Fukuoka, Japan, 1997); J. Non-Cryst. Solids* at press
[11] Perera D N and Harrowell P 1998 *Phys. Rev. Lett.* **81** 120
[12] Perera D N and Harrowell P 1998 A two dimensional glass: microstructure and dynamics of a 2D binary mixture *Proc. 3rd Int. Discussion on Relaxation in Complex Systems (Vigo, Spain, 1997); J. Non-Cryst. Solids* **235–237** 314
[13] Perera D N and Harrowell P 1998 Molecular dynamics simulations of a supercooled two dimensional binary mixture of soft discs: structure, stability and thermodynamics *Phys. Rev.* E submitted
[14] Perera D N and Harrowell P 1998 Relaxation dynamics and their spatial distribution in a two dimensional glass-forming binary mixture *Phys. Rev.* E submitted
[15] Hurley M M and Harrowell P 1995 *Phys. Rev.* E **52** 1694
[16] Evans D J and Morriss G P 1983 *Chem. Phys.* **77** 63
Evans D J and Morriss G P 1984 *Comput. Phys. Rep.* **1** 297
[17] Allen M P and Tildesley D J 1987 *Computer Simulations of Liquids* (Oxford: Oxford University Press)
[18] Foley M and Harrowell P 1993 *J. Chem. Phys.* **98** 5069
[19] Fredrickson G H and Andersen H C 1984 *Phys. Rev. Lett.* **53** 1244
Fredrickson G H and Brawer S A 1986 *J. Chem. Phys.* **84** 3351
Fredrickson G H 1991 *Annu. Rev. Phys. Chem.* **39** 149
[20] Alder B J and Wainwright T E 1970 *Phys. Rev.* A **1** 18
[21] Hurley M M and Harrowell P 1996 *J. Chem. Phys.* **105** 10 521
[22] Perera D N and Harrowell P 1998 *Phys. Rev. Lett.* **80** 4446
[23] Hurley M M and Harrowell P 1996
[24] Bendler J T and Shlesinger M F 1992 *J. Phys. Chem.* **96** 3970
[25] Perera D N and Harrowell P 1996 *Phys. Rev.* E **54** 1652